Supplemental Material for the manuscript LW12553

Weak localization in mesoscopic hole transport: Berry phases and classical correlations

Viktor Krueckl,[1] Michael Wimmer,[2] İnanç Adagideli,[3] Jack Kuipers,[1] and Klaus Richter[1]

[1]*Institut für Theoretische Physik, Universität Regensburg, D-93040 Regensburg, Germany*
[2]*Instituut-Lorentz, Universiteit Leiden, P.O. Box 9506, 2300 RA Leiden, The Netherlands*
[3]*Faculty of Engineering and Natural Sciences, Sabanci University, Istanbul 34956, Turkey*

(Dated: February 9, 2011)

In this supplement we provide additional information to our calculations on mesoscopic hole transport [1]. In Section A we compare the band-structure and Berry phases between the 4-band Hamiltonian used in [1] with the more general 8×8 Hamiltonian. In Section B we provide a derivation of Eq. (7) in [1]. In Section C we consider weak localization in 2-band and 4-band based models for HgTe cavities with spin-orbit interaction. Finally in Section D we provide parameters used in the calculation of [1].

A: 8-band versus 4-band Hamiltonian

The electronic structure of III-V semiconductors around the Γ-point can be described by various model Hamiltonians at different approximation levels containing a different number of bands [2]: The 8-band Kane Hamiltonian is composed of the s-like conduction band (CB) and the p-like valence band which splits into the heavy-hole (HH), the light-hole (LH) and the split-off (SO) band. The corresponding 8×8 matrix can be separated into two blocks like the 4×4 Hamiltonian used in [1], where one block is the time-inverse of the other block. In both of these 4×4 blocks all the bands are strongly coupled, leading to a bulk band-structure as shown in Fig. 1(a) for the bulk. Note that the HH band is slightly non-parabolic stemming from the spin-orbit induced repulsion between the

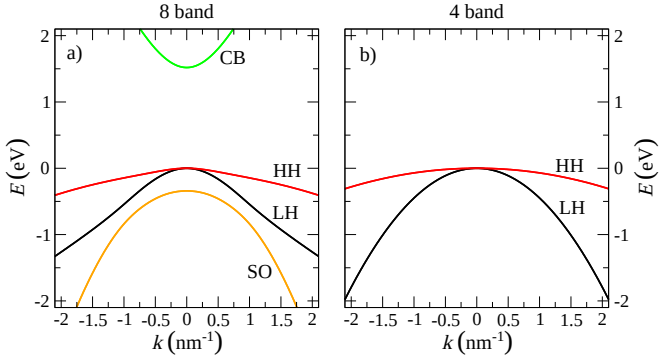

FIG. 1: (*Color online*) Comparison between the bulk band-structure given by the 8-band Kane model (a) and the 4-band Kohn-Luttinger model (b) in a bulk system. Material parameters are chosen to fit GaAs in an axial approximation.

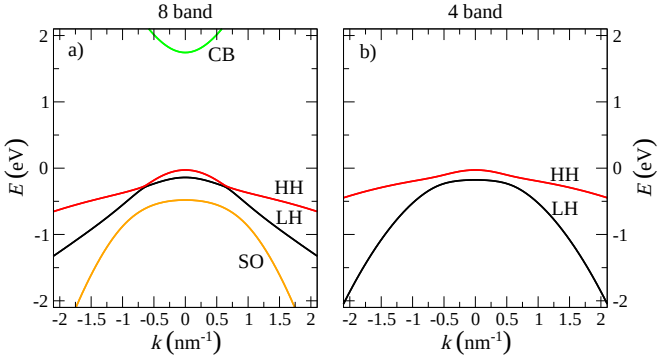

FIG. 2: (*Color online*) Comparison between the band-structure given by the 8-band Kane model (a) and the 4-band Kohn-Luttinger model (b) for a 5 nm quantum well in z-direction. Both show an anti-crossing between the HH and LH states leading to a pronounced Berry phase. Material parameters are chosen to fit GaAs in an axial approximation.

LH, CB and SO bands.

Neglecting remote bands results in the 4-band Kohn-Luttinger Hamiltonian. In the bulk, the eigensystem of this Hamiltonian simply leads to two parabolic bands,

$$E^{4\times4}_{\mathrm{LH,HH}} = -\frac{\hbar^2 k^2}{2m}(\gamma_1 \pm 2\gamma_2). \tag{1}$$

In order to introduce a confinement in z-direction (to describe a two-dimensional hole gas (2DHG)) the $\hat{k}_z$ operator is replaced by its expectation values ($\langle \hat{k}_z \rangle = 0$, $\langle \hat{k}_z^2 \rangle = (\pi/a)^2$ with a the quantum well width). This results in a shift of the maxima of the HH and the LH band, leading to an anti-crossing between the HH and LH states. This is the case for both models, the 8-band and the 4-band Hamiltonian, as shown in Fig. 2. Nevertheless the two models differ in the strength of this anti-crossing. The SO band of the 8-band model leads to a much narrower anti-crossing compared to the anti-crossing in the 4-band model.

The HH-LH coupling, visible as the anti-crossing, is reflected in the Berry phase of the HH band differing in the two models. Here we calculate the associated Berry vector potential

$$\mathcal{A}_\sigma(\boldsymbol{k}) = -\mathrm{i}\langle \psi_\sigma(\boldsymbol{k}) | \nabla_k \psi_\sigma(\boldsymbol{k}) \rangle\,, \tag{2}$$

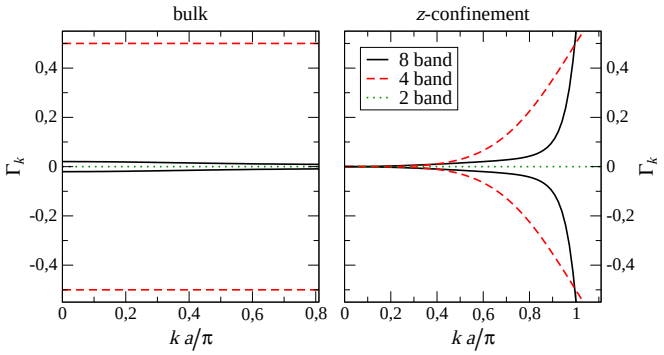

FIG. 3: (*Color online*) Comparison between the Berry phase effect on the HH subband in the 8-band Kane model (solid lines), the 4-band Kohn-Luttinger model (dashed) and a 2-band approximation (dotted). The left panel shows the Berry phase contribution for systems without confinement. If a confinement in z-direction is applied (here $a = 5$ nm) the interaction between HH and LH band leads to a similar Berry phase in both models. For a 2-band approximation the Berry phase is always zero.

from the plane wave solutions $\psi_\sigma(\boldsymbol{k})$ and extract the contribution

$$\Gamma_k = \mathcal{A}_{\mathrm{HH}}(\boldsymbol{k}) \cdot (-k_y, k_x)\,, \tag{3}$$

needed for the integration in momentum space to obtain the Berry phase [6].

For the system without confinement in z-direction the HH states exhibit only a very small Berry phase contribution for the HH states in the 8-band Hamiltonian while Γ_k in the 4-band Hamiltonian is clearly overestimated. This is shown in the left panel of Fig. 3 for different momenta.

On the contrary, the accuracy of the 4×4 model is much better for a two-dimensional system. The small confinement induced gap between HH and LH states leads to a Γ_k of comparable magnitude in both the 8-band and the 4-band Hamiltonian as shown in the right panel of Fig. 3. The remaining difference between the phases in the two models simply stem form the different transitions between the HH and LH character of the bands in the respective model. In the 8-band model this happens on a very small k scale, leading to an abrupt increase of Γ_k, while there is a smooth transition in the 4-band case associated with a smoother increase of Γ_k beginning at lower momenta.

In [1] we calculate the transport at the top of the HH band for small momenta. In this range, as shown in Fig. 3, the Berry phase contribution for both the 8- and the 4-band model is of similar magnitude, although their k-dependence differs. This similarity is why we use the 4-band model in our transport calculations.

B: Reflections at hard walls

In [1] we show how the Berry phase (Eq. (6) in [1]) due to the HH-LH interaction affects the quantum transport. In this context we assumed adiabatic transitions in momentum space. A similar effect occurs if the transition between different wave vectors is non-adiabatic as for the scattering at hard wall boundaries, as shown in the following.

The free solutions of the upper subblock $\hat{\mathcal{H}}_{\mathrm{U}}$ in Eq. (1) of [1] are given by the spinors

$$|\chi_{\mathrm{l}}(\tilde{k}_{\mathrm{l}},\varphi)\rangle = \left(1+\tfrac{\xi_{\mathrm{l}}^2}{3}\right)^{-1/2}\begin{pmatrix}1\\ \frac{1}{\sqrt{3}}\xi_{\mathrm{l}}(\tilde{k}_{\mathrm{l}})e^{-2\mathrm{i}\varphi}\end{pmatrix}, \tag{4a}$$

$$|\chi_{\mathrm{h}}(\tilde{k}_{\mathrm{h}},\varphi)\rangle = \left(1+\tfrac{\xi_{\mathrm{h}}^2}{3}\right)^{-1/2}\begin{pmatrix}1\\ \frac{1}{\sqrt{3}}\xi_{\mathrm{h}}(\tilde{k}_{\mathrm{h}})e^{-2\mathrm{i}\varphi}\end{pmatrix}, \tag{4b}$$

with the momentum dependent parameters

$$\xi_{\mathrm{l}}(\tilde{k}_{\mathrm{l}}) = 1-2\tilde{k}_{\mathrm{l}}-2\sqrt{1-\tilde{k}_{\mathrm{l}}+\tilde{k}_{\mathrm{l}}^2}, \tag{5a}$$

$$\xi_{\mathrm{h}}(\tilde{k}_{\mathrm{h}}) = 1-2\tilde{k}_{\mathrm{h}}+2\sqrt{1-\tilde{k}_{\mathrm{h}}+\tilde{k}_{\mathrm{h}}^2}, \tag{5b}$$

where $\tilde{k}_{\mathrm{l/h}} = \frac{\langle k_z^2\rangle}{k_{\mathrm{l/h}}^2}$. Assuming specular reflections we study an incoming wave (with angle φ_1) and an outgoing wave (with angle φ_2) consisting of a traveling HH and an evanescent LH part which both have to vanish at the hard wall boundary. Thus the two spinor components must obey

$$|\chi_{\mathrm{h}}(\varphi_1)\rangle + t_{\mathrm{h}}|\chi_{\mathrm{h}}(\varphi_2)\rangle + r_{\mathrm{l}}|\chi_{\mathrm{l}}(\varphi_1)\rangle + t_{\mathrm{l}}|\chi_{\mathrm{l}}(\varphi_2)\rangle = 0. \tag{6}$$

Due to current conservation the reflected HH amplitude is given by

$$t_{\mathrm{HH}\Uparrow}(\varphi) = \frac{\xi_{\mathrm{l}} - \xi_{\mathrm{h}}e^{-2\mathrm{i}\varphi}}{|\xi_{\mathrm{l}} - \xi_{\mathrm{h}}e^{-2\mathrm{i}\varphi}|}, \tag{7}$$

for the HH part of $\hat{\mathcal{H}}_{\mathrm{U}}$, where $\varphi = \varphi_2 - \varphi_1$. The result for $\hat{\mathcal{H}}_{\mathrm{L}}$ is the complex conjugate. For small $\xi_{\mathrm{h}}/\xi_{\mathrm{l}}$ one finds

$$\xi^{\mathrm{hw}} = \frac{\xi_{\mathrm{h}}}{\xi_{\mathrm{l}}} \approx -\frac{1}{4}\frac{\gamma_1+\bar{\gamma}}{\bar{\gamma}}\left(\frac{k_{\mathrm{h}}a}{\pi}\right)^2 - \\ -\frac{1}{16}\frac{\gamma_1^2+2\gamma_1\bar{\gamma}-2\bar{\gamma}}{\bar{\gamma}^2}\left(\frac{k_{\mathrm{h}}a}{\pi}\right)^4 + O\left(\left(\tfrac{k_{\mathrm{h}}a}{\pi}\right)^6\right). \tag{8}$$

Then the phase change in the HH reflection amplitude (7) is given by

$$\Gamma_{\mathrm{HH}\Uparrow}(\varphi) = \frac{1}{\mathrm{i}}\ln t_{\mathrm{HH}\Uparrow}(\varphi) \overset{\xi^{\mathrm{hw}}\ll1}{\simeq} \xi^{\mathrm{hw}}\sin 2\varphi\,. \tag{9}$$

This phase which additionally arises at a boundary reflection is incorporated in the semiclassical transmission amplitudes in a way similar to the Berry phase. This completes the derivation of Eq. (7) in [1].

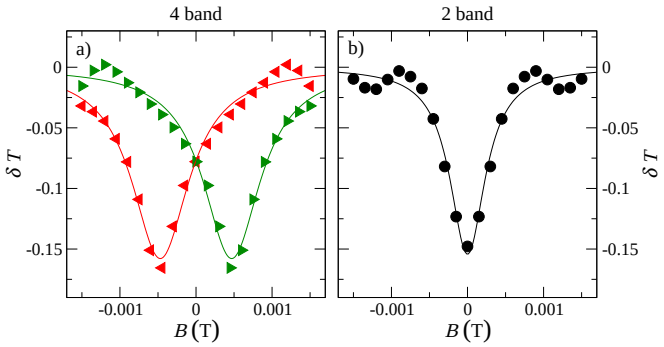

FIG. 4: (*Color online*) Weak localization in a circular quantum dot without bulk-inversion asymmetry ($\Delta = 0$, lead width $W = 50$ nm, main radius $R = 370$ nm). (a) The quantum dot modeled by the 4-band Hamiltonian shows a Berry phase induced shift between the weak-localization minima of the different subblocks. (b) The right panel shows the result for the effective 2-band Hamiltonian which cannot feature any Berry phase, and thus the localization minimum is located at $B = 0$. The symbols are given by numerics, and the corresponding lines are a fit with the weak-localization theory.

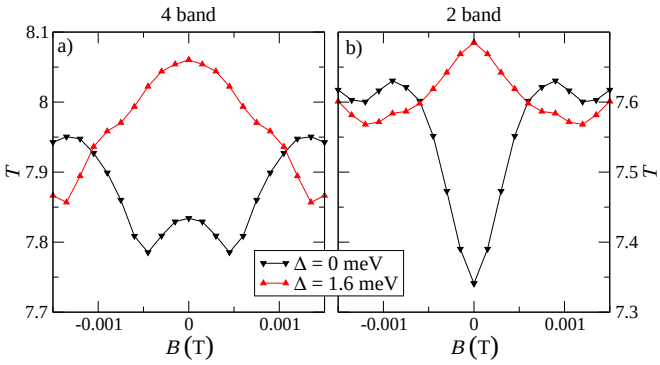

FIG. 5: (*Color online*) Weak localization in a circular quantum dot with and without bulk-inversion asymmetry (BIA) (lead width $W = 50$ nm, main radius $R = 370$ nm). (a) The left panel shows the results for the 4-band Hamiltonian. Without BIA (▼) the weak localization is splitted into a double-peak structure. With additional BIA (▲) the localization turns into a very broad anti-localization peak. (b) The right panel shows the result for the effective 2-band Hamiltonian which cannot feature any Berry phase, and thus the localization minimum without BIA is located at $B = 0$. The BIA also leads to anti-localization, but this still differs from the result with an additional Berry phase.

C: Weak localization in ballistic HgTe cavities

Quantum transport through a quantum dot based on the topological insulator HgTe [3] also shows the typical shifted weak localization correction similar to the one of the hole gas. In order to model the material we use the 4-band Hamiltonian [4]

$$H = \begin{pmatrix} M-(B+D)\boldsymbol{k}^2 & A(k_x+ik_y) & & -\Delta \\ A(k_x+ik_y) & -M+(B-D)\boldsymbol{k}^2 & \Delta & \\ & \Delta & M-(B+D)\boldsymbol{k}^2 & -A(k_x-ik_y) \\ -\Delta & & -A(k_x+ik_y) & -M+(B-D)\boldsymbol{k}^2 \end{pmatrix} \tag{10}$$

consisting of the heavy-hole and the conduction band. As material parameters we use the values in Table I with positive mass M leading to a system without a topological state. It can be shown that the Berry phase in HgTe is also very strong. Thus a weak localization calculation (based on Hamiltonian (10)) in the conducting region shows two split minima as depicted in Fig. 4(a). The result is very similar to the one for the 2DHG (Fig. 3(b) in [1]). The WL peak splitting depends again on the correlation between the enclosed area and the winding angle of the trajectories inside the cavity. On the other hand the bandstructure of HgTe outside the gap can be modeled by an effective 2-band Hamiltonian as is also frequently done for hole gases to reduce the 4-band to a 2-band model. In the following we restrict ourself on the electron conducting region for energies $E_F > M$. By Löwdin partitioning we get a new

A	B	C	D	M	Δ
354.5	−686	0	−512	10	1.6

TABLE I: Material parameters for HgTe (units in meV and nm)[5].

effective Hamiltonian

$$H = \left(M + \frac{\Delta^2}{2M}\right)\sigma_0 + \Delta\frac{A}{M}(k_x\sigma_x - k_y\sigma_y) + \frac{2A^2M + (B+D)(\Delta^2 - 4M^2)}{4M^2}\sigma_0 k^2. \tag{11}$$

This Hamiltonian is similar to that of an electron gas and thus all Berry phase effects have been removed from the initial 4-band version. Consequently the weak localization minimum for a transport calculation based on (11) is located at $B = 0$ as shown in Fig. 4(b). Note that even higher order terms do not introduce any Berry phase into the effective Hamiltonian (11). The Berry phase is hidden in the 2-band model in the momentum dependent basis. To recover the Berry phase effects, this basis would have to be properly accounted for in a transport calculation. This Berry phase however is completely omitted if one only considers the resulting effective two-band model (without basis transformation), as is usually done in the interpretation of weak localization measurements. In this case the weak localization signal is just given by a single Lorentzian-like minimum located at zero magnetic field as shown in Fig. 5(b). Thus the total transmission for both spin components differs strongly between the 4-band and the 2-band model (see Fig. 5(a,b)).

HgTe additionally exhibits a bulk-inversion asymmetry (BIA) which enters into the Hamiltonian as a spin-orbit coupling Δ. We also calculated the conductance through the circular quantum dot for a realistic BIA strength. The results show anti-localization as summarized for the 2-band and the 4-band Hamiltonian in Fig. 5. A comparison between the two calculations shows a noticeable difference in the 2-band and the 4-band model anti-localization. This indicates the rele-

vance of Berry phase effects even in the case of strong BIA spin-orbit interaction.

D: System parameters for the transport calculations

For the calculation of weak localization schown in Fig. 3(a-d) in [1] we used the following parameters:

GaAs in axial approximation $\gamma_1 = 6.85$, $\bar{\gamma} = 2.5$, $ka/\pi = 0.64$; Geometries (lengths in units of nm): a): 5 open modes per subblock, $R = 350, W = 40$, b): 5 open modes per subblock, $R = 200, W = 40$, c): 5 open modes per subblock, $R = 800, W = 40$, d): 15 open modes per subblock, $L = 2000, W = 120$. Averages taken over ~ 2000 energies and geometries (a-c) and ~ 1000 disorder configurations (d).

[1] V. Krueckl, M. Wimmer, I. Adagideli, J. Kuipers, and K. Richter, ??? **??**, ???? (???)

[2] R. Winkler, *Spin-orbit Coupling Effects in Two-Dimensional Electron and Hole Systems* (Springer, 2003).

[3] C. Brüne, A. Roth, E. G. Novik, M. König, H. Buhmann, E. M. Hankiewicz,W. Hanke, J. Sinova, and L.W. Molenkamp, Nature Physics **6**, 448 (2010).

[4] B. A. Bernevig, T. L. Hughes, and S.-C. Zhang, Science **314**, 1757 (2006).

[5] M. König, H. Buhmann, L. W. Molenkamp, T. Hughes, C.-X. Liu, X.-L. Qi, and S.-C. Zhang, J. Phys. Soc. Jpn. **77**, 031007 (2008).

[6] The relative phase of the states is chosen to be constant with respect to the major spinor entry at $k = 0$.